Colloid Polym Sci (2005) 283: 1349–1355
DOI 10.1007/s00396-005-1338-x

SHORT COMMUNICATION

Jian-She Hu
Bao-Yan Zhang
Mei Tian
Shi-Chao Ren
Deng-Yuan Guo

Mesomorphic properties of side-chain cholesteric liquid-crystalline elastomers

Received: 02 December 2004
Accepted: 22 March 2005
Published online: 22 June 2005

J.-S. Hu · B.-Y. Zhang (✉) · M. Tian
S.-C. Ren · D.-Y. Guo
Center for Molecular Science and Engineering, Northeastern University, Shenyang 110004
People's Republic of China
E-mail: baoyanzhang@hotmail.com

Abstract New monomer cholesteryl 4-(10-undecylen-1-yloxybenzoyloxy)-4′-ethoxybenzoate (M_1), crosslinking agent biphenyl 4,4′-bis(10-undecylen-1-yloxybenzoyloxy-*p*-ethoxybenzoate) (M_2) and a series of side-chain cholesteric elastomers were prepared. The chemical structures of the monomers and elastomers obtained were confirmed by element analyses, FT-IR, and ^{1}H NMR. The mesomorphic properties and thermal stability were investigated by differential scanning calorimetry, thermogravimetric analysis, polarizing optical microscopy, and X-ray diffraction measurements. The influence of the content of the crosslinking unit on the phase behavior of the elastomers was examined. $\mathbf{M_1}$ showed cholesteric phase, and $\mathbf{M_2}$ displayed nematic phase. The elastomers containing less than 12 mol% of the crosslinking units revealed reversible mesomorphic phase transition, wide mesophase temperature ranges, and high thermal stability.

Keywords Liquid crystalline elastomers · Cholesteric · Nematic · Smectic

Introduction

Research into liquid-crystalline elastomers (LCEs) with anisotropic properties has expanded rapidly [1–11], and in particular, LCEs with cholesteric structures have attracted considerable interest because of their unique properties and potential applications in numerous areas, especially in the fields of nonlinear optical materials and electro-optical materials etc. [12–16]. Cholesteric LCEs combine basic features of polymer elastomers with the anisotropy of physical properties of cholesteric LC. Consequently, cholesteric LCEs not only hold the entropic elasticity but also show reversible LC phase transitions on heating and cooling cycles. Compared with conventional LCEs, cholesteric LCEs show unusual piezoelectricity [17–23], tunable mirrorless lasing [24, 25], and photonics [26, 27] besides electro-optical and mechanical properties. Piezoelectricity of cholesteric LCEs, as a physical effect of polarization induced by mechanical deformation has been undeniable [20]. Cholesteric LCEs have the potential to act as a device that transforms a mechanical signal into an electric signal when stress is applied parallel to the cholesteric helix, thus they are considered as a candidate for the piezoelectric device. Therefore, it is necessary to synthesize various kinds of side-chain cholesteric LCEs to explore their potential applications.

In previous study, we reported the synthesis and properties of side-chain cholesteric LCEs derived from smectic and nonmesogenic crosslinking agent, respectively [28, 29]. In this study, a series of new side-chain cholesteric LCEs derived from nematic crosslinking agent were prepared. The mesomorphic properties, phase behavior and thermal stability of the monomers and elastomers obtained were investigated with differential scanning calorimetry (DSC), thermogravimetric analysis (TGA), polarizing optical microscopy (POM), and X-ray diffraction (XRD) measurements. The use of

nematic mesogenic crosslinking agent not only can induce cholesteric phase, but also should promote the formation of mesophases in the network and widen mesophase temperature range.

Experimental

Materials

Polymethylhydrosiloxane(PMHS, $\bar{M}_n = 700 - 800$) was purchased from Jilin Chemical Industry Co. Cholesterol was purchased from Henan Xiayi Medical Co. Undecylenic acid was purchased from Beijing Jinlong chemical Reagent Co., Ltd. 4,4′-Dihydroxybiphenyl (from Aldrich) was used as received. All solvents and reagents were purified by standard methods.

Measurements

The element analyses were carried out by using a Elementar Vario EL III (Elementar, Germany). FT-IR spectra were measured on a Perkin-Elmer spectrum One (B) spectrometer (Perkin-Elmer, Foster City, CA, USA). ^{1}H NMR spectra (300 MHz) were obtained with a Varian Gemini 300 spectrometer (Varian Associates, Palo Alto, CA, USA). Optical rotations were obtained on a Perkin-Elmer 341 polarimeter. Phase transition temperatures and thermodynamic parameters were determined by using a Netzsch DSC 204 (Netzsch, Germany) equipped with a liquid nitrogen cooling system. The heating and cooling rates were 10 °C/min. The thermal stability of the polymers under nitrogen atmosphere was measured with a Netzsch TGA 209C thermogravimetric analyzer. A Leica DMRX (Leica, Germany) POM equipped with a Linkam THMSE-600 (Linkam, England) hot stage was used to observe phase transition temperatures and analyze LC properties for the monomers and polymers through observation of optical textures. XRD measurements were performed with a nickel-filtered Cu-K_α radiation with a DMAX-3A Rigaku (Rigaku, Japan) powder diffractometer.

Synthesis of the monomers

The synthesis of the vinylic monomers is shown in Scheme 1. 4-(10-Undecylen-1-yloxy)benzoic acid (**1**) and 4-(hydroxyethoxy)benzoic acid (**2**) were synthesized according to the reported literature [29].

*4-(10-Undecylen-1-yloxybenzoyloxy)-4′-ethoxybenzoic acid (**3**)*

Compound **3** was prepared by reacting 4-(10-undecylen-1-yloxy)benzoyl chloride (32.4 g, 0.1 mol) with compound **2** (18.2 g, 0.1 mol) in the presence of 200 mL of tetrahydrofuran (THF) and 15 mL of *N*,*N*-dimethylformamide (DMF). The reaction mixture was refluxed for 17 h and cooled to room temperature, then filtered. After concentrating the filtrate, the product was pre-

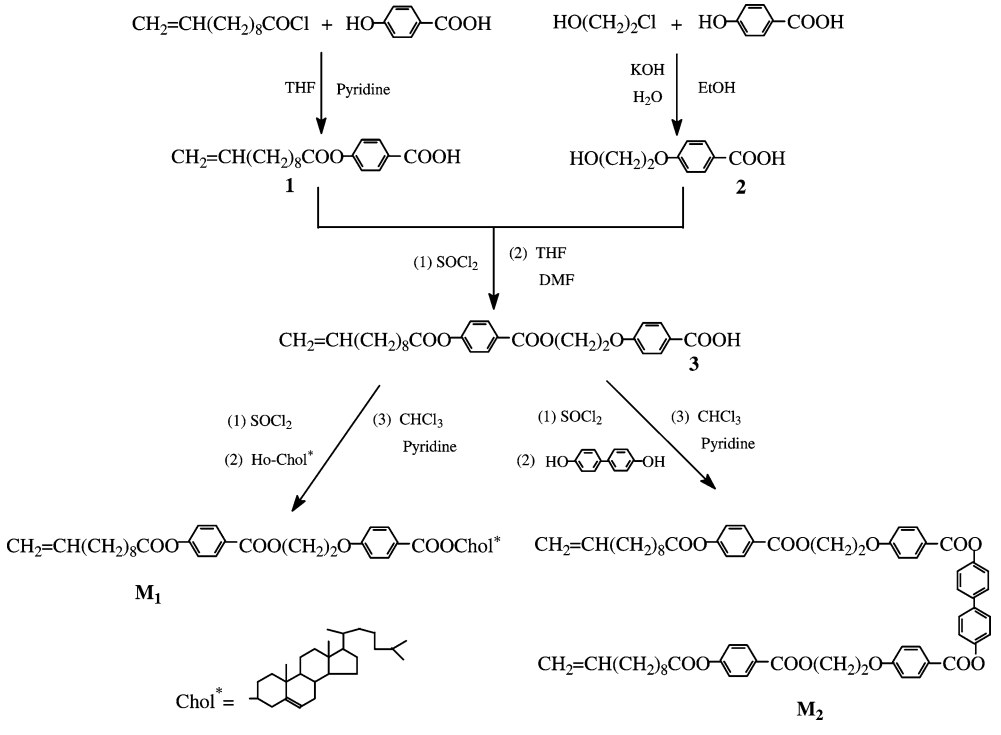

Scheme 1 Synthetic route of monomer and crosslinking agent

cipitated by adding water to the residue, and the crude product was obtained by filtration and recrystallized from ethanol. White crystal **3** was obtained. Yield 24.8 g (53%), melting point 123 °C.

Elemental analysis ($C_{27}H_{32}O_7$): calculated; C, 69.21%; H, 6.88%. Found: C, 69.32%; H, 7.11%.

IR (KBr): 3,076 (=C–H); 2,932, 2,855 (–CH_2–); 2,671, 2,564 (–COOH); 1,736, 1,675 (C=O); 1,607, 1,502 (Ar–), 1,257 cm^{-1} (C–O–C).

^{1}H NMR ($CDCl_3$, TMS), δ(ppm): 1.23 (s, 8H, –C H_2–); 1.27 (s, 2H, CH_2=CHCH_2C H_2–); 1.54 (m, 2H, –C H_2CH_2COO–); 1.95 (m, 2H, CH_2=CHC H_2–); 2.26 (m, 2H, –C H_2COO–); 4.45 (t, 2H, –C H_2O–); 4.73 (t, 2H, –COOC H_2–); 4.96 (dd, 1H, C H_2=CH–); 5.04 (dd, 1H, C H_2=CH–); 5.81 (m, 1H, CH_2=C *H*–); 6.97 (d, 2H, Ar–*H*); 7.19 (d, 2H, Ar–*H*); 7.93 (d, 2H, Ar–*H*); 8.03 (d, 2H, Ar–*H*); 10.9 (s, 1H, –COO *H*).

*Cholesteryl 4-(10-undecylen-1-yloxybenzoyloxy)-4′-ethoxybenzoate (***M$_1$***)*

Compound **3**(56.2 g, 0.12 mol) was reacted at 60 °C with 73 mL of thionyl chloride containing a few drops of DMF for 10 h, and then the excess thionyl chloride was removed under reduced pressure to give the corresponding 4-(10-undecylen-1-yloxybenzoyloxy)-4′-ethoxybenzoyl chloride. The acid chloride obtained (18.3 g, 0.05 mol) was dissolved in 20 mL of chloroform, and then added dropwise to a solution of cholesterol (19.4 g, 0.05 mol) in 4 mL of pyridine and 100 mL of chloroform. The mixture was refluxed for 15 h and cooled to room temperature, then filtered. After concentrating the filtrate, the crude product was precipitated by adding ethanol to the residue and recrystallized from chloroform/ethanol (1:1). Solid **M$_1$** was obtained. Yield 23.4 g (56%), $[\alpha]_D^{25}$ −1.4° (c=0.743, toluene).

Elemental analysis ($C_{54}H_{76}O_7$): calculated; C, 77.47%; H, 9.2%. Found: C, 77.21%; H, 9.02%.

IR (KBr): 3,076 (=C–H); 2,926, 2,853 (–CH_2–, –CH_3); 1,756 (C=O); 1,604, 1,507 (Ar–), 1,259 cm^{-1} (C–O–C).

^{1}H NMR ($CDCl_3$, TMS, δ, ppm): 0.63−2.39 [m, 59H, cholesteryl−*H* and –(C H_2)$_8$–]; 4.05 (m, 1H, –COOC *H*< in cholesteryl); 4.43 (t, 2H, –C H_2O–); 4.76 (t, 2H, –COOC H_2–); 5.01 (dd, 1H, ^2J1.6, $^3J_{cis}$10.3, C H_2=CH–); 5.05 (dd, 1H, ^2J1.6, $^3J_{trans}$17.3, C H_2=CH–); 5.35 (d, 1H,^3J6.5, =C *H*– in cholesteryl); 5.81 (ddt, 1H, $^3J_{cis}$10.3, $^3J_{trans}$17.3, ^3J6.3, CH_2=C *H*–); 6.86 (d, 2H, ^3J_o8.4, Ar–*H*); 7.16 (d, 2H, ^3J_o8.9, Ar–*H*); 7.92 (d, 2H, ^3J_o8.4, Ar–*H*); 7.98 (d, 2H, ^3J_o8.9, Ar–*H*).

*Biphenyl 4,4′-bis(10-undecylen-1-yloxybenzoyloxy-p-ethoxybenzoate) (***M$_2$***)*

4-(10-Undecylen-1-yloxybenzoyloxy)-4′-ethoxybenzoyl chloride (18.3 g, 0.05 mol) was dissolved in 15 mL of THF, and added dropwise to a solution of 4,4′-dihydroxybiphenyl (4.65 g, 0.025 mol) in 4 mL of pyridine and 80 mL of chloroform. The mixture was refluxed for 15 h and cooled to room temperature, then filtered. After concentrating the filtrate, the crude product was precipitated by adding ethanol to the residue. The obtained product was purified by recrystallization from acetic acid. Yield 17.9 g (66%), mp 116 °C.

Elemental analysis ($C_{66}H_{70}O_{14}$): calculated; C, 72.91%; H, 6.49%. Found: C, 72.65%; H, 6.58%.

IR (KBr): 3,074 (=C–H); 2,928, 2,857 (–CH_2–); 1,752 (C=O); 1,606, 1,502 (Ar–); 1,255cm^{-1} (C–O–C).

^{1}H NMR ($CDCl_3$, TMS, δ, ppm): 1.28 (s, 16H, –C H_2–); 1.33 (s, 4H, CH_2=CHCH_2C H_2–); 1.52 (m, 4H, –C H_2CH_2COO–); 1.94 (m, 4H, CH_2=CHC H_2–); 2.31 (m, 4H, –C H_2COO–); 4.37 (t, 4H, –C H_2O–); 4.80 (t, 4H, –COOC H_2–); 5.01 (dd, 2H, ^2J1.6, $^3J_{cis}$10.3, C H_2=CH–); 5.06 (dd, 2H, ^2J1.6, $^3J_{trans}$17.1, C H_2=CH–); 5.91 (ddt, 2H, $^3J_{cis}$10.3, $^3J_{trans}$17.1, ^3J6.5, CH_2=C *H*–); 6.91 (d, 4H, ^3J_o8.5, Ar–*H*); 7.18 (d, 4H, ^3J_o8.8, Ar–*H*); 7.22–7.56 (m, 8H, Ar–*H*); 7.95 (d, 4H, ^3J_o8.5, Ar–*H*); 8.02 (d, 4H, ^3J_o8.8, Ar–*H*).

Synthesis of the elastomers

The elastomers **P$_2$**–**P$_7$** were synthesized by the same methods. For the synthesis of **P$_3$**, the monomers **M$_1$**, **M$_2$**, and **PMHS**, as shown in Table 1, were dissolved in 40 mL of freshly distilled toluene. The mixture was heated to 65 °C under nitrogen and anhydrous conditions, and then 2 mL of THF solution of H_2PtCl_6 catalyst (5 mg/mL) was injected with a syringe. The progress of the hydrosilylation reaction, monitored by the Si–H (2,166 cm^{-1}) stretch intensity, went to completion as indicated by IR. The elastomer **P$_3$** was obtained and purified by several reprecipitations from toluene solution into methanol, and then dried *in vacuum*.

IR (KBr): 2,934–2,853 (−CH_3, –CH_2–); 1,764, 1,737 (C=O); 1,604, 1,502 (Ar–); 1,300–1,000 cm^{-1} (Si–O–Si, C–Si and C–O–C).

Table 1 Polymerization and yields

Polymer	Feed (mmol)			M_2^a (mol%)	Yield (%)
	PHMS	M_1	M_2		
P_1	1	7.00	0.00	0	79
P_2	1	6.86	0.14	2	77
P_3	1	6.48	0.27	4	73
P_4	1	5.98	0.52	8	74
P_5	1	5.50	0.75	12	76
P_6	1	5.17	0.91	15	75
P_7	1	4.68	1.17	20	72

[a]Molar fraction of M_2 based on (M_1 + M_2)

Results and discussion

Syntheses

The synthetic routes for the target monomers are shown in Scheme 1. **M_1** and **M_2** were synthesized by reacting 4-(10-undecylen-1-yloxybenzoyloxy)-4′-ethoxybenzoyl chloride with cholesterol and 4,4′-dihydroxybiphenyl, respectively, in in the presence of chloroform and pyridine. IR spectra of **M_1** and **M_2** showed characteristic bands at 1,756, 1,605 and 1,505 cm^{-1} attributed to ester C=O and aromatic C=C stretching band. ^1H NMR spectra of **M_1** showed multiplet at 7.98–6.86, 5.81–5.01, and 4.76–0.63 ppm corresponding to aromatic protons, olefinic protons, and methyl and methylene protons, respectively. ^1H NMR spectra of **M_2** showed multiplet at 8.02–6.91, 5.91–5.01, and 4.80–1.28 ppm corresponding to aromatic protons, olefinic protons, and methylene protons, respectively. The spectra of **M_1** and **M_2** suggest high purity as confirmed by the element analyses.

The elastomers **P_2**–**P_7** were prepared by hydrosilylation reaction in toluene, using H_2PtCl_6 as catalyst at 65 °C. Yields and detailed polymerization are summarized in Table 1. The obtained elastomers were insoluble in toluene, xylene, DMF, chloroform etc. IR spectra of**P_2**–**P_7** showed the complete disappearance of Si–H stretching band at 2,165 cm^{-1}. Characteristic Si–O–Si stretching bands appeared at 1,300–1,000 cm^{-1}. In addition, the absorption bands of ester C=O and aromatic still existed.

Thermal analysis

The thermal properties of **M_1**, **M_2** and **P_1**–**P_7** were investigated by DSC. Their phase transition temperatures and corresponding enthalpy changes, obtained on the second heating and the first cooling scan, are summarized in Tables 2 and 3, respectively. All phase transitions were reversible and do not change on repeated heating and cooling cycles. The phase transition temperatures determined by DSC were consistent with POM observation results. Representative DSC curves of **M_1** are presented in Fig. 1.

Differential scanning colorimetry curves of **M_1** only showed a cholesteric–isotropic phase transition and an isotropic–cholesteric phase transition at 163 and 160 °C, respectively; a melting transition and crystallization process did not appear. DSC heating curves of **M_2** showed a melting transition at 117 °C and a nematic to isotropic phase transition at 239 °C. On cooling scans of **M_2**, an isotropic–nematic phase transition at 235 °C and crystallization temperature appeared at 102 °C.

Table 2 Phase transition temperatures of monomers

Monomer	Transition temperature in °C (corresponding enthalpy changes in J g^{-1}) (heating/cooling)
M_1	K–Ch163(1.8)I/I160(0.9)Ch–K
M_2	K117(4.6) N239(1.0)I/I235(0.8)N102(4.1)K

K solid, *Ch* cholesteric, *N* nematic, *I* isotropic

Table 3 Thermal properties of polymers

Polymer	T_g (°C)	T_i (°C)	ΔH_1 (J g^{-1})	ΔT^a	T_d^b (°C)
P_1	25	251	2.1	226	325
P_2	28	246	1.4	218	328
P_3	29	232	1.0	203	328
P_4	33	221	0.8	188	329
P_5	35	204	0.7	169	332
P_6	41	–	–	–	333
P_7	46	–	–	–	337

[a]Mesophase temperature ranges (T_i– T_g)
[b]Temperature at which 5% weight loss occurred

Differential scanning colorimetric thermograms of **P_1**–**P_5** showed a glass transition and a LC phase to isotropic transition, respectively. In general, low levels of chemical crosslinking did not significantly affect the LC behavior of the elastomers, and reversible LC phase transitions can be observed because of enough molecular motion. In contrast, high levels of chemical crosslinking had a strong influence on the LC behavior of the elastomers, it might cause LC phase to disappear due to the depression of LC orientational order. Therefore, DSC curves of **P_6** and **P_7** only showed a glass transition. Figure 2 shows the effect of the concentration of crosslinking units on the phase transition temperatures of the elastomers.

In general, chemical crosslinking imposes additional constraints on the motion of chain segments, reduces free volume, and causes an increase in T_g. Taking the chemical crosslinking effect into account, T_g is given by

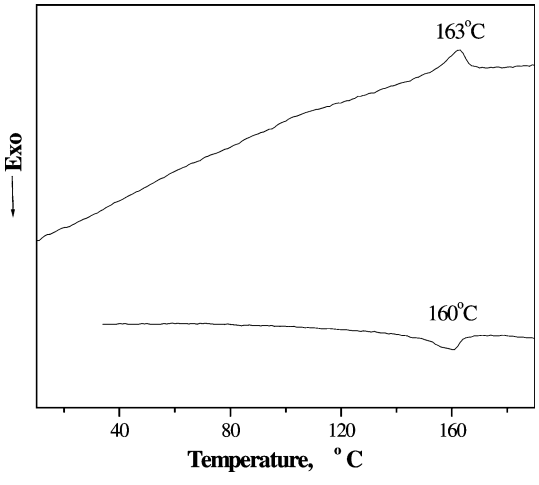

Fig. 1 DSC thermograms of M_1

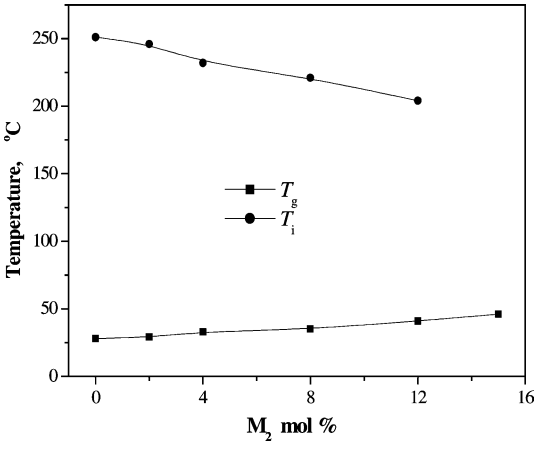

Fig. 2 Effect of M_2 content on the phase transition temperatures of the elastomers

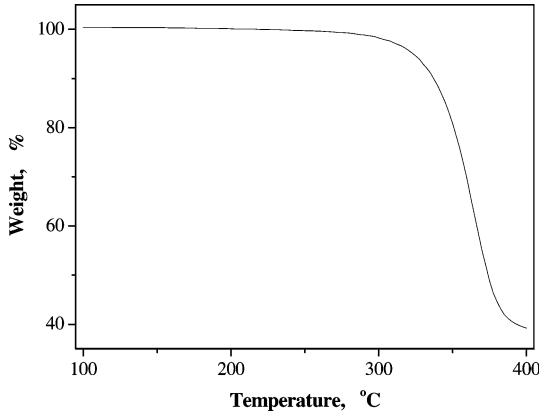

Fig. 3 Thermogravimetric analysis curve of $\mathbf{P_2}$

$$T_g = T_{go} + K_x\rho_x$$

where T_g and T_{go} are the glass transition temperatures of crosslinked and uncrosslinked polymers, K_x is constant, and ρ_x is the crosslink density. It was clearly seen that T_g of $\mathbf{P_1}$–$\mathbf{P_7}$ increased from 25 °C to 46 °C when the concentration of crosslinking units increased from 0 mol% to 20 mol%.

The chemical crosslinking affected T_i in two ways for $\mathbf{P_2}$–$\mathbf{P_5}$. On one hand, the flexible crosslinking chains acted as diluent and caused a decrease in the T_i; on the other hand, chemical crosslinking could prevent the motion and orientation of mesogenic molecule in the vicinity of the crosslinking sites and did not favor the formation of mesogenic orientation order in the networks. According to Table 3, T_i of $\mathbf{P_1}$–$\mathbf{P_5}$ decreased from 251 °C to 204 °C, and ΔH decreased from 2.1 J g^{-1} to 0.7 J g^{-1} when the concentration of crosslinking units increased from 0 mol% to 12 mol%. This indicates that the LC order reduces from $\mathbf{P_1}$ to $\mathbf{P_5}$. In addition, $\mathbf{P_1}$–$\mathbf{P_5}$ displayed wider mesophase temperature ranges (ΔT). Moreover, ΔT decreased from 226 °C to 169 °C with increasing concentration of the crosslinking unit because T_i decreased and T_g increased.

Thermogravimetric analysis results of the polymers are shown in Table 3. Typical TGA curve of $\mathbf{P_2}$ is shown in Fig. 3. TGA results showed that the temperatures at which 5% weight loss occurred (T_d) were greater than 320 °C for $\mathbf{P_1}$–$\mathbf{P_7}$, respectively, this displays high thermal stability of the synthesized polymers and LC phase. Moreover, T_d of $\mathbf{P_1}$–$\mathbf{P_7}$ increased with increasing concentration of the crosslinking units.

Texture analysis

The optical textures of the monomers and polymers obtained were studied by POM with hot stage. POM results showed that $\mathbf{M_1}$ exhibited enantiotropic cholesteric phase, and $\mathbf{M_2}$ exhibited nematic phase on heating and cooling cycles. When $\mathbf{M_1}$ was heated to 67 °C, mesomorphic properties occurred, the typical cholesteric oily-streak texture and reflection color appeared at 88 °C. The reflection color changed from red, yellow, green to blue with temperature from 88 °C to 154 °C. Texture disappeared at 167 °C. When the isotropic state was cooled to 166 °C, the focal-conic appeared, if a mechanical field was superimposed on the sample at that time, for example, slight shearing the melt would cause macroscopic orientation of the cholesteric domains, and the focal-conic texture transformed to oily-streak texture, which is a typical characteristic of cholesteric LC. Optical textures of $\mathbf{M_1}$ are shown in Fig. 4a–c. When $\mathbf{M_2}$ was heated to 115 °C, nematic thread and schlieren texture appeared gradually, and mesomorphic behavior disappeared at 245 °C. When the isotropic state was cooled to 243 °C, the nematic droplet and schlieren texture appeared, and crystallized at 91 °C. Optical textures of $\mathbf{M_2}$ are shown in Fig. 5.

The uncrosslinked polymer $\mathbf{P_1}$ exhibited smectic broken focal-conic texture, and expected cholesteric phase did not appear, the reason being that the polymer chains hinder the formation of the helical supramolecular structure of the mesogens. The elastomers $\mathbf{P_2}$–$\mathbf{P_4}$ exhibited cholesteric Grabdjean texture, and cholesteric texture of$\mathbf{P_5}$ was not easily identified because of the higher viscoelasticity. This indicates that the introduction of the nematic unit into the polymer can induce the cholesteric phase. Moreover, $\mathbf{P_6}$ displayed stress-induced birefringence although DSC curve showed no LC phase to isotropic phase transition. This is similar to those described by Mitchell [30]. However, $\mathbf{P_7}$ showed only elasticity with no other texture; this is consistent with the results obtained by DSC. Optical textures of $\mathbf{P_1}$ and $\mathbf{P_3}$ are shown in Fig. 6a, b.

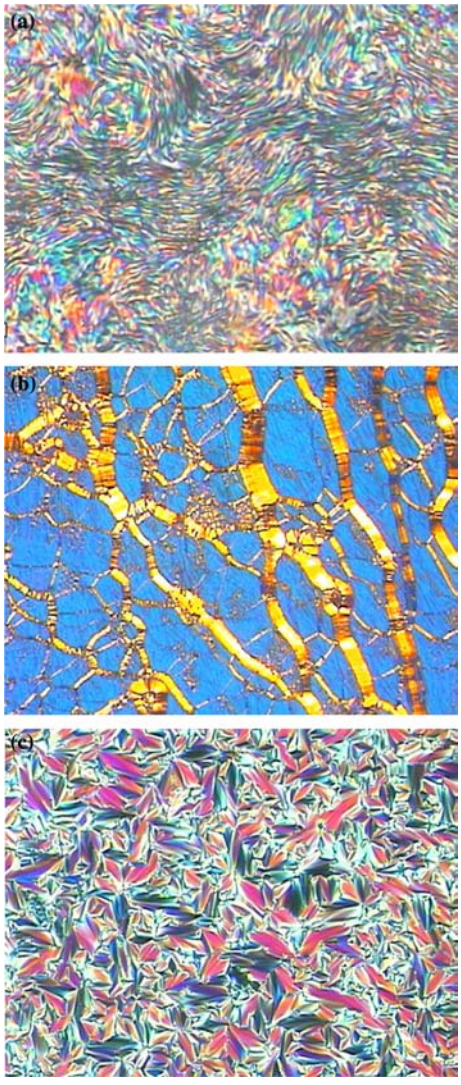

Fig. 4 Optical textures of $\mathbf{M_1}$ (200×): **a** spiral texture on heating to 114 °C; **b** oily-streak texture on heating to 159 °C; **c** focal-conic texture on cooling to 155 °C

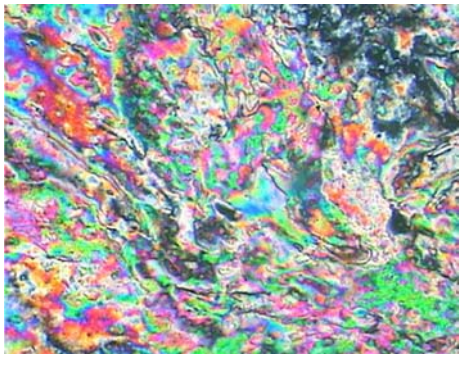

Fig. 5 Thread textures of $\mathbf{M_2}$ on heating to 164 °C (200×)

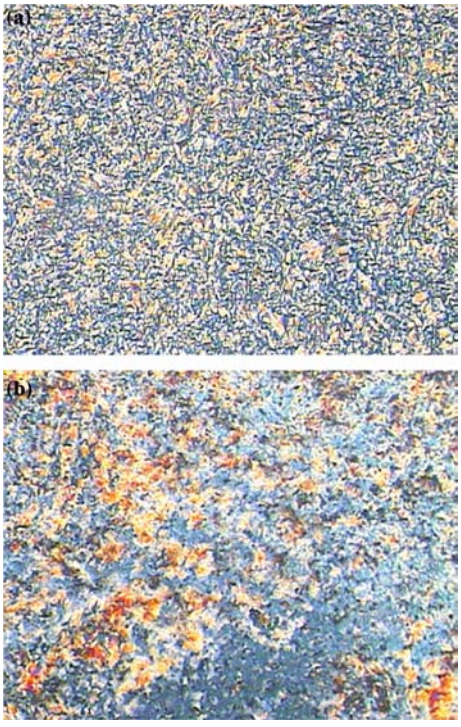

Fig. 6 Optical textures of polymers (200×): **a** broken focal-conic texture of P_1 on cooling 231 °C; **b** Grandjean texture of P_3 on cooling 203 °C

XRD analysis

X-ray diffraction studies were carried out to obtain more detailed information on the mesogenic structure and type. In general, a sharp and strong peak at low angle ($1° < 2\theta < 4°$) in small-angle X-ray scattering (SAXS) curves and a strong broad peak associated with lateral packing at $2\theta \approx 20°$ can be observed in wide-angle X-ray diffraction (WAXD) curves for smectic structure. For nematic structure, no peak appears in SAXS curve, but in WAXD curve a broad peak at $2\theta \approx 20°$ can also be observed. For cholesteric structure also, no peak appeared in SAXS curve, however, we discovered a broad peak occurring about at $2\theta = 16–18°$ [31–33]. For $\mathbf{P_1}$, a sharp peak associated with the smectic layers appeared at $2\theta = 2.2°$ in SAXS curves, however, a sharp peak did not appear in SAXS curves, and broad peaks were observed at about $2\theta = 16.3–17.1°$ in WAXD curves for $\mathbf{P_2}$–$\mathbf{P_6}$. Moreover, broad peaks were more and more diffuse, and peak intensity reduced with increasing the crosslink density, this indicates the decrease of LC order from $\mathbf{P_1}$ to $\mathbf{P_5}$.

Conclusions

In this study, a series of new side-chain cholesteric LCEs containing cholesteryl 4-(10-undecylen-1-yloxybenzoyl-

oxy)-4′-ethoxybenzoate and biphenyl 4,4′-bis(10-undecylen-1-yloxybenzoyloxy-*p*-ethoxybenzoate) were synthesized and characterized. $\mathbf{M_1}$ showed cholesteric oily-streak texture and focal-conic texture; $\mathbf{M_2}$ showed nematic thread texture and schlieren texture. All the obtained polymers showed very wide mesophase temperature ranges and high thermal stability. The elastomers containing less than 12 mol% of crosslinking units showed elasticity and reversible mesomorphic phase transition on heating and cooling cycles. For $\mathbf{P_1}$–$\mathbf{P_5}$, the glass transition temperature increased, and clearing temperature and mesophase temperature ranges decreased with increasing concentration of crosslinking unit.

Acknowledgements The authors are grateful to National Natural Science Fundamental Committee of China, HI-Tech Research and development program (863) of China, Science and Specialized Research Fund for the Doctoral Program of Higher Education of China, and Science and Technology Bureau of Shenyang for financial support of this work.

References

1. Hikmet RAM, Lub J (1992) Macromolecules 25:4194
2. Hikmet RAM, Lub J, Higgins JA (1993) Polymer 34:1736
3. Jahromi S, Lub J, Mol GN (1994) Polymer 35:622
4. Warner M, Terentjev EM (1996) Prog Polym Sci 21:853
5. Frich D, Economy J (1997) J Polym Sci A Polym Chem 35:1061
6. Hsu CS, Chen HL (1999) J Polym Sci A Polym Chem 37:3929
7. Callau L, Reina JA, Mantecòn A (2002) J Polym Sci A Polym Chem 40:3893
8. Bonet J, Callau L, Reina JA Galià M, Cádiz V (2002) J Polym Sci A Polym Chem 40:3883
9. Callau L, Reina JA, Mantecón A (2003) J Polym Sci A Polym Chem 41:3384
10. Ribera D, Serra A, Mantecón A (2003) J Polym Sci A Polym Chem 41:2521
11. Tian YQ, Kong XX, Nagase Y, Iyoda T (2003) J Polym Sci A Polym Chem 41:2197
12. Yang DK, West JL, Chien LC, Doane WJ (1994) J Appl Phys 76:1331
13. Broer DJ, Lub J, Mol GN (1995) Nature 378:467
14. Bunning TJ, Kreuzer FH (1995) Trends Polym Sci 3:318
15. Peter PM (1998) Nature 391:745
16. Sapich B, Stumpe J, Kricheldorf HR (1998) Macromolecules 31:1016
17. Hirschmann H, Meier W, Finkelmann H (1992) Makromol Chem Rapid Commun 13:385
18. Pleiner H, Brand HR (1993) J Phys II 3:1397
19. Terentjev EM (1993) Euro Phys Lett 23:27
20. Pelcovits RA, Meyer RB (1995) de Physique II 5:877
21. Brehmer M, Zentel R (1994) Mol Cryst Liq Cryst 243:353
22. Kelly SM (1995) J Mater Chem 5:2047
23. Terentjev EM, Warner M (1998) Eur Phys J B 8:595
24. Finkelmann H (2001) Adv Mater 13:1069
25. Schmidtke J, Stille W, Finkelmann H (2003) Phys Rev Lett 90:083902
26. Cicuta P, Tajbakhsh AR, Terentjev EM (2002) Phys Rev E 65:051704
27. Bermel PA, Warner M (2002) Phys Rev E 65:056614
28. Hu JS, Zhang BY, Guan Y (2004) J Polym Sci A Polym Chem 42:5262
29. Zhang BY, Hu JS, Wang Y, Qian JH (2003) Polym J 35:476
30. Mitchell GR, Davis FJ, Ashman A (1987) Polymer 28:639
31. Hu JS, Zhang BY, Jia YG, Chen S (2003) Macromolecules 36:9060
32. Zhang BY, Hu JS, Jia YG, Du BG (2003) Macromol Chem Phys 204:2123
33. Hu JS, Zhang BY, Sun K, Li QY (2003) Liq Cryst 30:1267